Metal-induced energy transfer for live cell nanoscopy

Alexey I. Chizhik[1]*, Jan Rother[2], Ingo Gregor[1], Andreas Janshoff[2] and Jörg Enderlein[1]*

The discovery of Förster resonance energy transfer (FRET)[1] has revolutionized our ability to measure inter- and intramolecular distances on the nanometre scale using fluorescence imaging. The phenomenon is based on electromagnetic-field-mediated energy transfer from an optically excited donor to an acceptor. We replace the acceptor molecule with a metallic film and use the measured energy transfer efficiency from donor molecules to metal surface plasmons[2] to accurately deduce the distance between the molecules and metal. Like FRET, this makes it possible to localize emitters with nanometre accuracy, but the distance range over which efficient energy transfer takes place is an order of magnitude larger than for conventional FRET. This creates a new way to localize fluorescent entities on a molecular scale, over a distance range of more than 100 nm. We demonstrate the power of this method by profiling the basal lipid membrane of living cells.

In 1948, Theodor Förster published his first paper[1], in which he described the mechanism of resonant energy transfer (later named after him) between a fluorescent donor molecule and an absorbing acceptor molecule. He deduced that the transfer efficiency depends on the sixth power of the distance between donor and acceptor. This strong dependence between transfer efficiency and distance made Förster resonant energy transfer (FRET) one of the most powerful fluorescence-based methods in biophysical and physicochemical research for measuring distances on a molecular scale. Although recent years have seen a burst of new super-resolution methods in fluorescence microscopy[3–6], their resolving power is typically still one order of magnitude less than that achievable with FRET. A limitation of FRET is that the distance range for which it is applicable is typically limited to up to ∼10 nm. Another complication is the nontrivial dependence of the FRET efficiency on the mutual orientations of donor and acceptor molecules, which makes a quantitative conversion of FRET efficiency into accurate distance challenging as soon as the donor and acceptor molecules do not rotate freely and rapidly (compared to the fluorescence lifetime).

It has long been known that placing a fluorescent molecule in the vicinity of a metal quenches its fluorescence emission and decreases its fluorescence lifetime. This was first predicted by Edward Purcell in a seminal short note in 1946 (ref. 7). From a physics point of view, the mechanism behind this phenomenon is similar to that of FRET: energy from the excited molecule is transferred, via electromagnetic coupling, into plasmons of the metal, where energy is either dissipated or re-radiated as light. This fluorophore–metal interaction was extensively studied in the 1970s and 1980s (ref. 2), and a quantitative theory developed on the basis of semiclassical quantum optics[8,9]. The achieved quantitative agreement between experimental measurement and theoretical prediction was excellent.

Here, we show that the metal-induced energy transfer (MIET) can be used to localize fluorescent molecules along one dimension with nanometre accuracy. A first proof-of-principle study was

given in ref. 10, but the general idea has found little attention to date. The core idea is that the MIET accelerates the return of excited fluorescent molecules to their ground state, which manifests itself as a shortening of their fluorescence lifetime[11–13]. Owing to the fact that the energy transfer rate is dependent on the distance of a molecule from the metal layer, the fluorescence lifetime can be directly converted into a distance value (Fig. 1a). The theoretical basis for the success of this conversion is the perfect quantitative understanding of MIET[12,14]. It is important to emphasize that the energy transfer from the molecule to the metal is dominated by the interaction of the molecule's near-field with the metal and is thus a thoroughly near-field effect, similar to FRET. However, due to the planar geometry of the metal film, which acts as the acceptor, the distance dependency of the energy transfer efficiency is much weaker than the sixth power of the distance, which leads to a monotonous relation between lifetime and distance over a size range between zero and 100–200 nm above the surface.

We demonstrate the power of MIET by mapping the basal membrane of living cells with nanometre accuracy. The method does not require any hardware modification to a conventional fluorescence-lifetime imaging microscope (FLIM)[15,16], thus preserving its full lateral resolution. As a biological model system we chose three adherent cell lines: MDA-MB-231 human mammary gland adenocarcinoma cells and A549 human lung carcinoma cells, which are able to form metastasis *in vivo* models, and MDCK II from canine kidney tissue as a benign epithelial cell line. MIET imaging also allows cell motility to be monitored using time-elapsed imaging of the cell–substrate distance. In this way we can follow the motion of MDA-MB-231 cells over the surface with an axial resolution of 3 nm. We also monitored the spread of single MDCK-II cells by visualizing the various stages of adhesion from initial contact to the formation of lamellipodia. Knowledge of the precise cell–substrate distance as a function of time and location with unprecedented resolution provides a new means with which to quantify cellular adhesion and locomotion, as is required for a deeper understanding of fundamental biological processes such as cell differentiation, tumour metastasis and cell migration.

Figure 1b illustrates the experimental set-up, which comprises a conventional confocal microscope equipped with an objective lens (numerical aperture, 1.49), a pulsed excitation light source (20 MHz repetition rate, 50 ps pulse width, wavelength range 450–800 nm, 1 mW average power per nm; Fianium) and a time-correlated single-photon counting (TCSPC) module (HydraHarp, PicoQuant). The only additional requirement for MIET, when compared to conventional FLIM, is the presence of a thin semitransparent 20 nm gold film deposited on the glass cover slide supporting the sample. See Supplementary section 'Experimental set-up' for further details.

We applied MIET to map the cell–substrate distance of living cells. The cells were stained with a membrane-staining fluorophore (Cell Mask Deep Red plasma membrane stain, Invitrogen), which

[1]III. Institute of Physics, Georg August University, 37077 Göttingen, Germany, [2]Institute of Physical Chemistry, University of Göttingen, Tammannstrasse 6, 37077 Göttingen, Germany. *e-mail: chizhik@physik3.gwdg.de; enderlein@physik3.gwdg.de
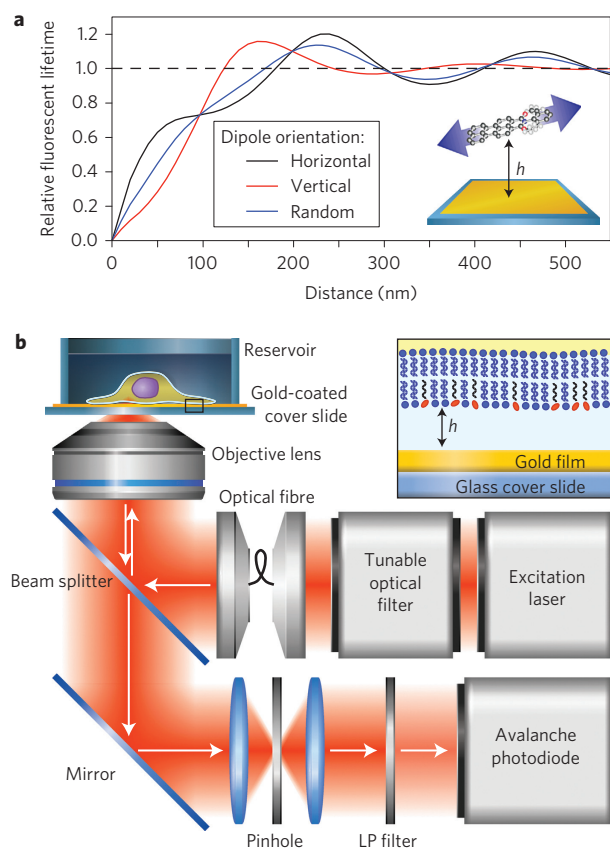
Figure 1 | Metal-induced fluorescence lifetime modification. a, Calculated dependence of fluorophore lifetime on its axial position over the metal film. Curves are calculated for an emission wavelength of 650 nm and a gold film thickness of 20 nm deposited on the glass cover slide. **b**, Scheme of the experimental set-up. LP, long pass.

Figure 2 | Fluorescence lifetime imaging. a,b, Simultaneously acquired fluorescence intensity (**a**) and lifetime (**b**) images of the basal membrane of living MDA-MB-231 cells grown on a gold-covered glass substrate, acquired with a standard confocal microscope.

emits photons in the deep red region of the visible spectrum. Using fluorescence interference contrast (FLIC) microscopy, it has been shown that the average distance of the basal membrane from the substrate typically varies between 20 and 100 nm depending on cell type[17], which is far below the diffraction-limited axial resolution of a confocal microscope. To keep the cells in physiological conditions, the microscope was equipped with an incubator, which kept the temperature constant at 37 °C. The cells were grown directly on a gold-coated glass substrate (20 nm gold evaporated on a glass cover slide with 150 μm thickness). Further details of the sample preparation can be found in Supplementary section 'Cell culture and staining'. FLIM images were acquired every 5 min with a field of view of 70×70 μm² (175×175 scan positions). As the apical cell membrane is at least 500 nm away from the substrate, only dye molecules within the basal membrane were efficiently excited and detected.

Figure 2a,b presents examples of the collected fluorescence intensity and lifetime images of the basal membrane of MDA-MB-231 cells, respectively. Because the variation of the fluorescence intensity is not only dependent on the metal-induced quenching, but also on the homogeneity of labelling, we exclusively used the lifetime information for reconstructing a three-dimensional map of the basal membrane. Computation of the local height of the basal membrane above the gold film was accomplished by using the theoretically calculated dependence of the fluorescence lifetime on the distance of a fluorophore from the metal film (Fig. 1a). The model takes into account all the details of the optical properties of the glass/gold substrate (thickness and wavelength-dependent complex-valued
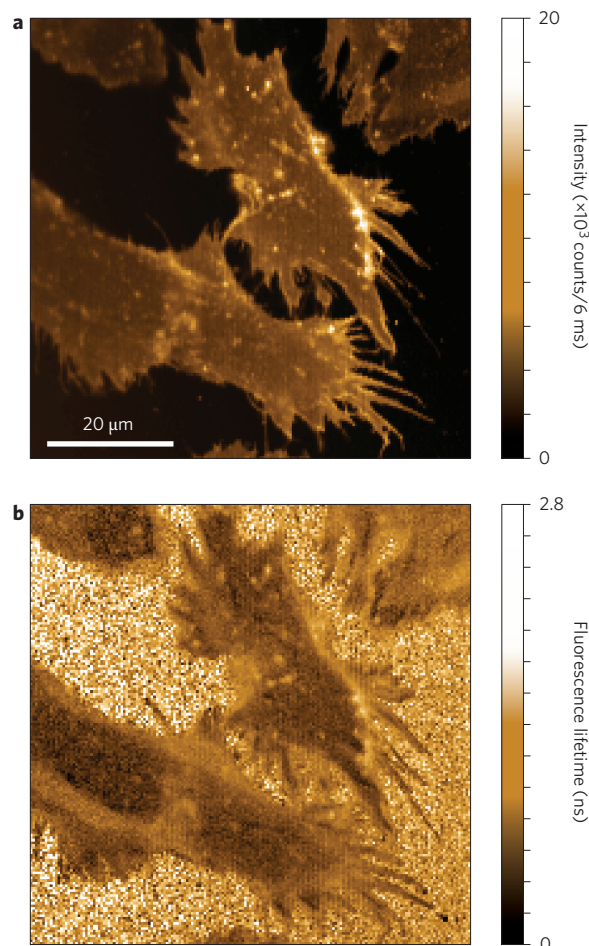
refractive index of the metal film; refractive index of the cover slide), as well as the photophysics of the used dye (emission spectrum, dye orientation with respect to the substrate). The dye orientation within the cell membrane was checked by defocused imaging[18] and was found to be random without any preferential orientation (Supplementary section 'Defocused imaging'). The distance–lifetime dependence, as calculated for the experimental conditions used in our experiment, is shown in Fig. 1a. We checked the accuracy of our model calculations by applying MIET to map the surface profile of a dye-coated glass lens with a well-known height profile (Supplementary section 'Verification of the theoretical model with a test sample').

Whereas the three-dimensional reconstruction of the membrane profile is recalculated solely from the lifetime image of the sample, the intensity distribution is used for discriminating, in the lifetime images, the membrane fluorescence against the background. Regions with no cells are difficult to identify from the lifetime images alone, as the lifetime values become exceedingly scattered at low signal-to-noise ratios. We eliminated such patches by removing areas where the fluorescence intensity did not exceed the background level. Finally, to ensure that the membrane stain had not internalized during the experiment, we carried out FLIM imaging of the intracellular compartments, which did not yield any detectable fluorescence signal.

Figure 3a presents a three-dimensional reconstruction of the basal membrane of MDA-MB-231 cells calculated from the lifetime
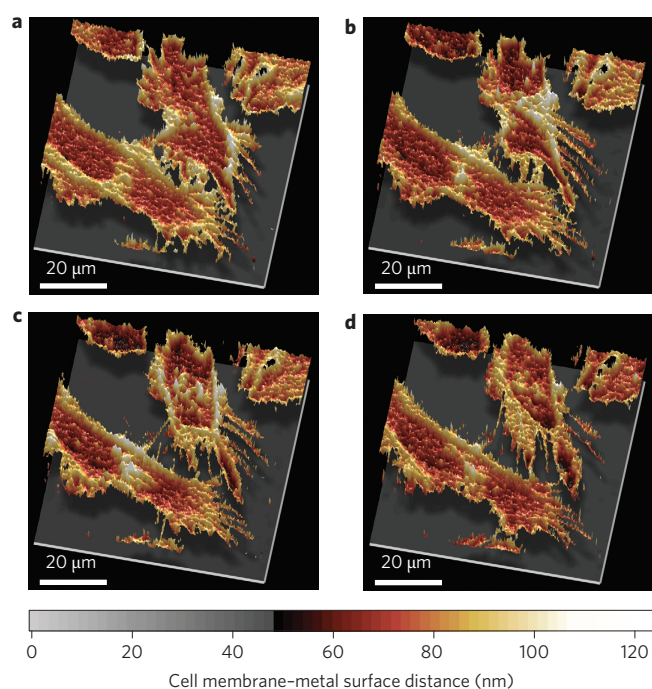
Figure 3 | Three-dimensional reconstruction of the basal cell membrane. Three-dimensional profiles computed from fluorescence lifetime images recorded over 40 min. See Supplementary section 'Full series of images' for full series of images.
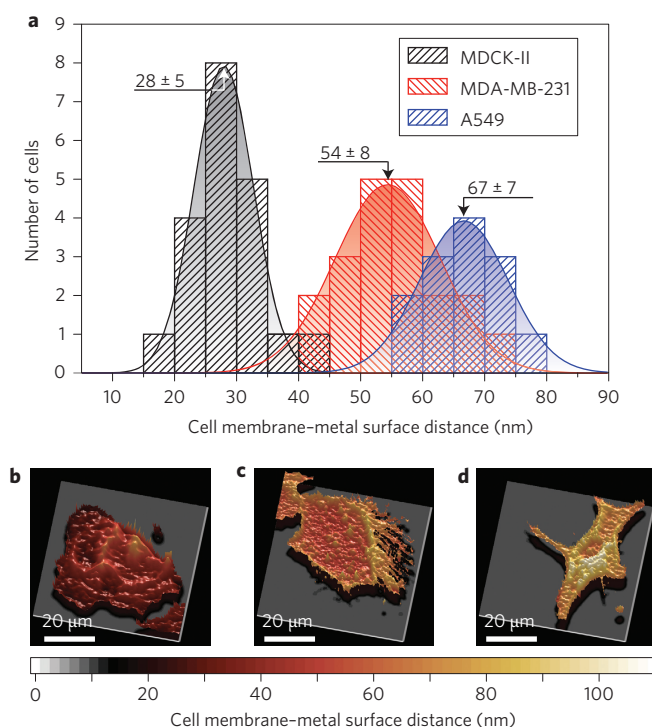

Figure 4 | Comparison of three cell lines. a, Average distance of basal membrane from the gold surface for MDA-MB-231, A549 and MDCK-II cell lines. Solid curves show the fit to the experimental data with a Gaussian function. **b–d,** Exemplary three-dimensional reconstructions of the basal membrane of the MDCK-II (**b**), MDA-MB-231 (**c**) and A549 (**d**) cells. Scale bars, 20 μm. For a better comparison, all images are normalized to the same scale.

images shown in Fig. 2. The local cell–substrate distance varies between 50 and 100 nm, whereby at the edges the cells exhibit a higher distance from the surface. The average cell–substrate distance is in very good agreement with the recently reported results of Wegener and colleagues, who reported 27 nm for MDCK-II and 87 nm for NIH 3T3 fibroblasts. Differences in cell–substrate distance for different cell types can occur due to variations in adhesion strength and in the secretion of extracellular matrix proteins by the cells themselves. To follow the temporal dynamics of the cell–substrate distance, we recorded a time-lapse series of fluorescence lifetime and intensity images at 5 min intervals. Figure 3a–d shows every second image of the series (see Supplementary section 'Full series of images' for the full series). The three-dimensional maps allow the cell motion to be followed over time with 200 nm lateral (as defined by the confocal microscope) and 3 nm axial resolution (see below). Although the cell–substrate distance at each lateral position changes over time, the average distance remains the same over the full measurement time. We found that the tumour cells display a larger cell–substrate distance in the periphery compared to the centre, where they firmly adhere to the gold surface.

A comparison of the three cell lines (MDA-MB-231, A549 and MDCK-II) with respect to the average distance of the basal membrane from the gold surface, as well as example MIET images, are provided in Fig. 4. We found excellent agreement with data obtained previously using FLIC microscopy, which showed that MDCK-II cells are extremely close to the surface (near 27 nm) (ref. 19). Note that MDCK-II cells are benign epithelial cells, whereas the other cell lines are cancerous and show a higher invasiveness/motility. This might be inferred from the higher cell–substrate distances of 54 ± 8 nm (MDA-MB-231) and 67 ± 7 nm (A549). We also investigated the spreading behaviour of MDCK-II cells (Supplementary section 'Spreading of MDCK-II cells'). Generally, the spreading process of adherent cells can be divided into three distinct temporal phases. The first phase is characterized by the formation of initial bonds between adhesion molecules and molecules of the extracellular matrix (ECM). This process of tethering is followed by the second phase, which comprises the initial cell spreading, which is driven by actin polymerization that forces the cell surface area to increase by drawing membrane from a reservoir of folded regions and blebs. The third phase encompasses recruitment of additional plasma membrane from the internally stored membrane buffer and extension of lamellipodia to occupy a larger area. By using MIET imaging we could monitor the individual phases by visualizing the cell–substrate distance as a function of time (Supplementary Figs 5 and 6). The MIET imaging shows that the initial contact of the cell is characterized by concentric areas, with alternating distance from the surface. The occupied area increases with time and, eventually, lamellipodia occur at the border of the cells that have close contact with the gold surface.

To estimate the resolution of the recorded images, we calculated the standard deviation of cell–substrate distance. For the acquired series of images, the resolution of the axial distance (determined with MIET) varies between 3 nm (at nearly 10×10^3 to 15×10^3 counts per pixel) and 4 nm (at nearly 5×10^3 to 10×10^3 counts per pixel), depending on the local signal-to-noise ratio. This substantially exceeds the precision of most existing techniques currently used for axial imaging. To prevent fast photobleaching of the sample, we used a moderate excitation power and acquisition time. However, as the resolution is determined by the signal-to-noise ratio of the recorded fluorescence decay curves, a further increase in precision can be achieved by collecting more fluorescence signal. A detailed analysis of the influence of photon statistics on axial resolution can be found in the Supplementary Information. With our current instrument, the MIET image acquisition speed is limited by the scan speed of our TCSPC confocal scanning microscope, which was sufficient to follow the relatively

slow motion of the cell membrane. Using a FLIM imaging system based on time-gated cameras or phase fluorometry, the acquisition speed can be increased by several orders of magnitude.

Although, in this Letter, we have focused on the application of MIET to the mapping of the membrane of a living cell, which shows its versatility, relative technical simplicity, and its potential for life-science applications, the potential scope of applications of MIET is much greater. The size range over which MIET works nicely bridges (and complements) the realm of conventional FRET and all the recently developed super-resolution imaging techniques. Although MIET has to rely on a perfect theoretical understanding of the fluorophore–metal interaction, which is certainly more involved than that of FRET, this is no serious obstacle in the current age of powerful desktop computers. In contrast to FRET, the infamous orientation-factor problem is greatly relaxed because one has to know only the relative orientation of one species of fluorescent molecules with respect to the planar metal film. Moreover, in contrast to FRET, one needs to label only one site of a sample with one species of fluorophore, instead of double-labelling with a donor and acceptor. MIET is exceedingly simple to set up and neither requires modification of the FLIM system nor preparation of complex sample substrates. Coating glass cover slides with a thin metal film is the only prerequisite of the technique. Thus, the technical simplicity of MIET will allow its application in a wide range of studies where nanometre resolution is required. We envisage that combining it with ideas from super-resolution microscopy techniques based on photoswitching and high-precision localization of single molecules will enable the resolution of inter- and intramolecular distances with nanometre precision. It may thus develop into an experimental tool that has similar power to FRET.

References

1. Förster, Th. Zwischenmolekulare energiewanderung und fluoreszenz. *Ann. Phys.* **437,** 55–75 (1948).
2. Drexhage, K. H. Interaction of light with monomolecular dye layers. *Prog. Opt.* **12,** 163–232 (1974).
3. Hell, S. W. Strategy for far-field optical imaging and writing without diffraction limit. *Phys. Lett. A* **326,** 140–145 (2004).
4. Rust, M. J., Bates, M. & Zhuang, X. Sub-diffraction-limit imaging by stochastic optical reconstruction microscopy (STORM). *Nature Methods* **3,** 793–795 (2006).
5. Betzig, E. *et al.* Imaging intracellular fluorescent proteins at nanometer resolution. *Science* **313,** 1642–1645 (2006).
6. Hess, S. T., Girirajan, T. P. K. & Mason, M. D. Ultra-high resolution imaging by fluorescence photoactivation localization microscopy. *Biophys. J.* **91,** 4258–4272 (2006).
7. Purcell, E. M. Spontaneous emission probabilities at radio frequencies. *Phys. Rev.* **69,** 681 (1946).
8. Lukosz, W. & Kunz, R. E. Light emission by magnetic and electric dipoles close to a plane interface. I. Total radiated power. *J. Opt. Soc. Am.* **67,** 1607–1615 (1977).
9. Chance, R. R., Prock, A. & Silbey, R. Molecular fluorescence and energy transfer near interfaces. *Adv. Chem. Phys.* **37,** 1–65 (1978).
10. Colyer, R. A., Lee, C. & Gratton, E. A novel fluorescence lifetime imaging system that optimizes photon efficiency. *Microsc. Res. Tech.* **71,** 201–213 (2008).
11. Chizhik, A. I. *et al.* Probing the radiative transition of single molecules with a tunable microresonator. *Nano Lett.* **11,** 1700–1703 (2011).
12. Chizhik, A. I. *et al.* Electrodynamic coupling of electric dipole emitters to a fluctuating mode density within a nanocavity. *Phys. Rev. Lett.* **108,** 163002 (2012).
13. Chizhik, A. I., Gregor, I. & Enderlein, J. Quantum yield measurement in a multicolor chromophore solution using a nanocavity. *Nano Lett.* **13,** 1348–1351 (2013).
14. Enderlein, J. Single-molecule fluorescence near a metal layer. *Chem. Phys.* **247,** 1–9 (1999).
15. Winckler, P., Jaffiol, R., Plain, J. & Royer, P. Nonradiative excitation fluorescence: probing volumes down to the attoliter range. *J. Phys. Chem. Lett.* **1,** 2451–2454 (2010).
16. Berndt, M., Lorenz, M., Enderlein, J. & Diez, S. Axial nanometer distances measured by fluorescence lifetime imaging microscopy. *Nano Lett.* **10,** 1497–1500 (2010).
17. Braun, D. & Fromherz, P. Fluorescence interferometry of neuronal cell adhesion on microstructured silicon. *Phys. Rev. Lett.* **81,** 5241–5244 (1998).
18. Patra, D., Gregor, I. & Enderlein, J. Image analysis of defocused single-molecule images for three-dimensional molecule orientation studies. *J. Phys. Chem. A* **108,** 6836–6841 (2004).
19. Heitmann, V., Reiss, B. & Wegener, J. The quartz crystal microbalance in cell biology: basics and applications. *Chem. Sens. Biosens.* **5,** 303–338 (2007).

Author contributions

A.I.C., J.R., A.J. and J.E. conceived and designed the experiments. A.I.C. and J.R. performed the experiments. A.I.C., J.R. and J.E. analysed the data. A.I.C., J.R., I.G., A.J. and J.E. contributed materials/analysis tools. A.I.C., J.R., A.J. and J.E. wrote the paper.

Additional information

Supplementary information is available in the online version of the paper. Reprints and permissions information is available online at www.nature.com/reprints. Correspondence and requests for materials should be addressed to A.I.C. and J.E.

Competing financial interests

The authors declare no competing financial interests.